Check for updates

Coarse-grained molecular dynamics simulations of nanoplastics interacting with a hydrophobic environment in aqueous solution†

Lorenz F. Dettmann, [ID] [a] Oliver Kühn [ID] [ab] and Ashour A. Ahmed [ID] *[ab]

Nanoplastics (NPs) are emerging threats for marine and terrestrial ecosystems, but little is known about their fate in the environment at the molecular scale. In this work, coarse-grained molecular dynamics simulations were performed to investigate nature and strength of the interaction between NPs and hydrophobic environments. Specifically, NPs were simulated with different hydrophobic and hydrophilic polymers while carbon nanotubes (CNTs) were used to mimic surface and confinement effects of hydrophobic building blocks occurring in a soil environment. The hydrophobicity of CNTs was modified by introducing different hydrophobic and hydrophilic functional groups at their inner surfaces. The results show that hydrophobic polymers have a strong affinity to adsorb at the outer surface and to be captured inside the CNT. The accumulation within the CNT is even increased in presence of hydrophobic functional groups. This contribution is a first step towards a mechanistic understanding of a variety of processes connected to interaction of nanoscale material with environmental systems. Regarding the fate of NPs in soil, the results point to the critical role of the hydrophobicity of NPs and soil organic matter (SOM) as well as of the chemical nature of functionalized SOM cavities/voids in controlling the accumulation of NPs in soil. Moreover, the results can be related to water treatment technologies as it is shown that the hydrophobicity of CNTs and functionalization of their surfaces may play a crucial role in enhancing the adsorption capacity of CNTs with respect to organic compounds and thus their removal efficiency from wastewater.

1 Introduction

Plastics are synthetic or semi-synthetic organic materials that contain mostly polymers as the main component. They are lightweight, corrosion-resistant and inexpensive materials with a wide range of applications. The downside of their durability are the problems associated with plastic waste and plastic debris in the environment. Plastic debris can disintegrate into smaller particles, even under ambient conditions.[1] Plastic particles that are smaller than a few millimeters in size are commonly known as microplastics and particles smaller than 1000 nm are known as nanoplastics (NPs).[2] These particles are widespread in the environment, including the oceans[3] and freshwater in Europe,[4] North America,[5] and Asia.[6] In marine ecosystems, plastic waste do not only cause aesthetic problems, but it can be also digested by organisms that mistake it for food.[7] 80% of the plastics in the marine wastes come from

land.[8] It was estimated that there may be 4 to 23 times more microplastics on land than in the ocean and that soil alone may contain more microplastics than the oceans.[9] In terrestrial systems, a primary entry point for microplastics is the agro-ecosystem, which is connected to the wide application of plastic mulch and sewage sludge.[10–13]

In agricultural ecosystems, various noxious substances, like persistent organic pollutants, or heavy metals can be adsorbed on plastic particles. Thereby, plastic particles can act as vectors for such environmental contaminants.[14] In general, transformations of NPs *via* homo- and hetero-aggregation could lead to advective flow transport, sedimentation, photo- and biodegradation, and/or sediment entrapment might occur.[15,16]

Estimation of NPs in the environment requires very sensitive and selective analytical techniques to detect the different types of NPs. These techniques would have to be sensitive towards particle sizes in the nanometer range and to concentrations down to nanograms per liter. Regarding the NPs investigation in soil, none of the published methods, such as vibrational spectroscopy or chromatography seems to be ideally suitable to detect these very small plastic particles. Regarding the spectroscopic measurements, the background fluorescence of organic matter or pigments of some polymers can strongly interfere with the spectra of interest, making them

[a]*University of Rostock, Institute of Physics, Albert-Einstein-Str. 23-24, D-18059 Rostock, Germany. E-mail: ashour.ahmed@uni-rostock.de*

[b]*University of Rostock, Department of Life, Light and Matter (LLM), Albert-Einstein-Str. 25, D-18059 Rostock, Germany*

† Electronic supplementary information (ESI) available. See DOI: 10.1039/d1ra04439g

unidentifiable.[17] Moreover, soil components can form relatively stable aggregates which may enclose plastic particles.[18] Ongoing modifications and combinations of methods, however, may help to enhance the currently very limited data in this field of research.[19]

Carbon nanotubes (CNTs) are macromolecules formed by sheets of graphene. They are characterized by a very high surface area, low density, high mechanical resistance, strong hydrophobicity and severe biodegradation.[20] Due to their unique physicochemical properties, CNTs have a wide range of technological applications.[21] This includes their use in the fields of water treatment and agricultural sector. In agricultural ecosystems, CNTs were used as nanosensors for various tasks involving detection and release of toxic substances to regulate plant growth and also to increase the life of fruits after harvest.[22–27] But also some toxic effects have been recorded for CNTs in soil and specifically in the agricultural sector.[28,29]

In a more fundamental study, Hyung and Kim[30] investigated the adsorption behavior of standard humic and fulvic acids to multi-walled carbon nanotubes (MWCNTs). Based on the Freundlich model, they found that there is a positive linear correlation between adsorption capacity and amount of aromatic group content. Ateia *et al.*[31] studied the adsorption process of the same humic and fulvic acids on MWCNTs and also found a linear correlation between adsorption constants and aromaticity (aromatic content) of a specific molecular system. In addition, they pointed to the dependence of the adsorption on the degree of oxidation and carboxylic acidity of the considered organic molecules. In a metastudy, Engel and Chefetz[32] evaluated a large set of data to quantitatively validate the correlation between aromatic content of dissolved organic matter and its adsorption to CNTs. The result has been negative, *i.e.* no correlation was observed. This contradiction with earlier work on specific cases was explained by the complexity and heterogeneity of dissolved organic matter and different CNTs characteristics.

While there is a huge number of literature covering interactions between NPs[33–35] or CNTs[30,31,36–38] with organic compounds, no studies are addressing the interaction between NPs and CNTs, although both chemical compounds might coexist, especially in the terrestrial environment. Moreover, CNTs provide a simple model system for studying the interaction of NPs with hydrophobic surfaces and cavities, the latter being an abundant motif in macromolecular soil organic matter particles.[39,40] Specific functional groups present in these macromolecules can easily be added to the CNTs and their effect, *e.g.*, on NPs binding can be quantified. Therefore, our objective is to introduce a molecular level understanding for the interaction of NPs with CNTs, which not only addresses this particular system but it should also mimic aspects of the interaction of NPs with soil organic matter. It should be noted that polymers in confined environments were investigated extensively throughout the last years.[41–47] Such models are not only a classical problem in polymer physics,[48] but also of interest because of their connection to biological processes like DNA packing in capsids[49] or chromosome separation during cell division.[50] In most of the investigations, entropic effects, chain formation or segregation of multiple chains are in the main focus.

In the present contribution, coarse-grained molecular dynamics (CGMD) as an effective approach to describe polymers and CNTs[51–54] will be used to model and simulate the behavior and interactions between NPs (unbranched polymer chains) and CNTs (bare and decorated with functional groups) in the presence of water. The overarching goals are (i) to introduce CGMD as an efficient tool for studying NP in the environmental context and (ii) to show the value of the generic model of functionalized CNTs, which captures essential aspects of the interaction of NPs with functional groups and hydrophobic cavities in situations where the actual atomistic information remains elusive due to complexity of composition and structural heterogeneity.

The rest of the paper is organized as follows. A detailed description of the modeling approach and computational details is presented in the next section. Then, the simulation results of different model systems are discussed. Finally, conclusions concerning the most important outcomes are presented.

2 Methods

2.1 Molecular modeling

The present study focuses on three different model systems. First, NPs in water will be studied to establish a relation between the number of monomer units and the radius of gyration in absences of CNTs. Second, the CNT is included to investigate its interaction with the NPs. Third, the CNTs are functionalized with organic groups to investigate the effect of the modified hydrophobicity of CNTs on the interaction between NPs and CNTs.

2.1.1 NPs in water. Polyethylene (PE), polypropylene (PP) and polystyrene (PS) are among the most abundant macro- and micro-plastics in marine and soil ecosystems.[11,55–59] Therefore, in the present study we modeled NPs by considering PE, PP and PS. Furthermore, polyethylene oxide (PEO) as a hydrophilic polymer was considered as well to take into account the hydrophobicity/hydrophilicity effect. Specifically, NPs were modeled as unbranched polymer chains, based on the MARTINI model for polymers.[60–63] The mapping schemes between the atomistic and the coarse-grained representations are introduced in Fig. 1a. For every polymer type, chains with different number of monomers N were considered, ranging from 5 up to 45 (for PEO), 200 (for PE), 350 (for PP) and 114 (for PS). These maximum chain lengths cover approximately the same range for the radius of gyration, R_g. Polymers were put into the center of cubic boxes. Each simulation box contains one single polymer. The length of one box vector was chosen depending on the number of monomers for each polymer: 50 Å for $N \leq 10$, 100 Å for $N \leq 30$ and 150 Å for $N > 30$. The boxes were filled with water particles with a density of about 1 g cm^{-3} using the Packmol software.[64] In the MARTINI model, one particle combines four atomistic water molecules.

2.1.2 NPs with CNTs in water. To explore the interaction between NPs and CNTs, different setups involving either PEO, PE, PP and PS of the previous section and a single CNT in water were considered. The coarse-grained CNT model was constructed by the "Open Carbon Nanotubes for the MARTINI Model" tool.[65] Exemplarily, a length of 100 Å and a diameter of
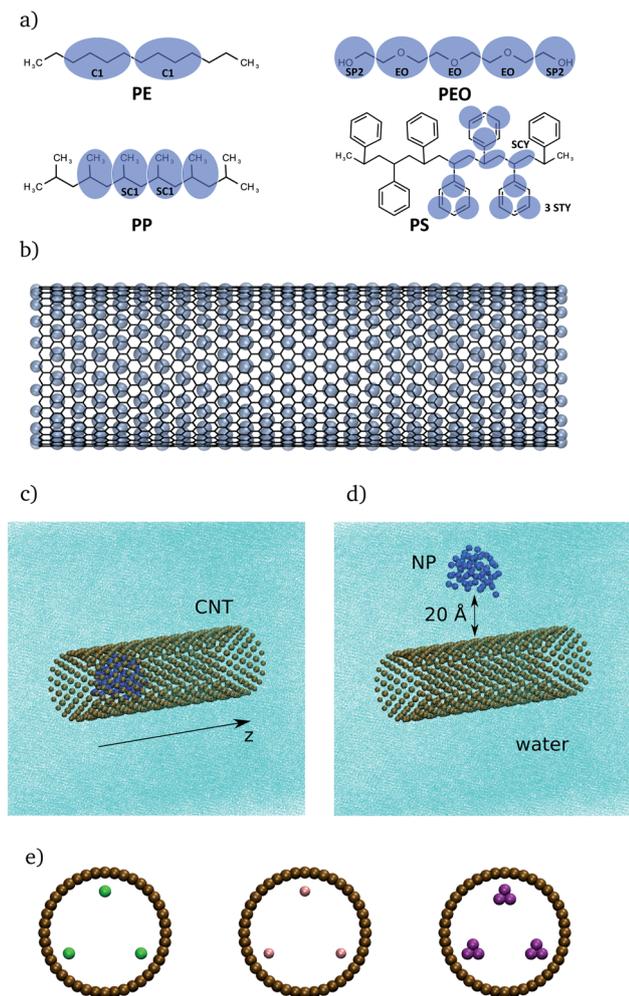
Fig. 1 (a): Illustration of PE, PEO, PP and PS models. The black lines correspond to the atomistic and the blue circles to the coarse-grained representation of the polymers. (b) Atomistic (black) and coarse-grained (blue) representation of the CNT. Two different starting configurations for PE, inside (c) and outside (d) the CNT. (e) Front view of CNTs with three functional groups, placed in the middle of these CNTs. The green beads (left) represent alkane chains (A), the pink beads (middle) represent carboxylic acid groups (CA) and the purple beads (right) represent phenyl groups (PH).

30 Å was chosen. A comparison of the coarse-grained and atomistic representation is shown in Fig. 1b. For each NP-CNT model, CNT was placed at the center of the simulation box, with box dimensions of 140 Å × 140 Å × 240 Å. Afterwards, one polymer was added into the constructed box. Then, the box containing the NP-CNT molecular system was filled with water, having a density of about 1 g cm^{-3}. For each NP-CNT model, each polymer had two different initial configurations. First, the polymers were placed inside the CNT at approximately one quarter of the CNT's length (see Fig. 1c). Second, the polymers were placed in water at about 20 Å distance from the outer wall of the CNT (see Fig. 1d). For each polymer, different chain lengths were considered based on their average R_g values in water, i.e. 6, 7, 8, 9, and 10 Å. With four different polymers (PE, PP, PS and PEO), five different chain lengths and two starting configurations for each chain, in total, 40 NP-CNT systems were

investigated. All initial configurations were chosen in a way that the polymers go through configurations of interest with sufficient duration time.

2.1.3 NPs with functionalized CNTs in water. To modify the hydrophobicity of the CNTs of the previous section, functional groups were introduced by attaching them to the inner walls of CNTs. The functional groups were inserted at the center of CNTs and kept fixed in position. Here, three different abundant soil organic matter functional groups are modeled, namely the nonpolar alkane chain (A) and phenyl group (PH) as well as the polar carboxylic acid group (CA).[66-71] Three groups of each type were added to the CNT (see their arrangement in Fig. 1e). To keep the model simple only one type of functional group was considered at the same time and all three functional groups are symmetrically arranged. For each polymer type, the case $R_g = 7$ Å was selected. For this value motion of the polymer through the CNT would be possible, at least in principle. For each NP-CNT system, polymers were initially placed inside the CNT at one quarter of its length. The boxes of NP-CNT systems were filled with water, with the same water density, and box dimensions as used in the previous section. Eventually, with four different polymers (PE, PP, PS and PEO) and three different functional groups (A, CA and PH), 12 NP-CNT systems were considered.

2.2 Computational details

MARTINI force field[60] based coarse-grained molecular dynamics simulations were performed using the GROMACS software package (version 2019.04).[72] The use of this coarse-graining approach has the advantages of accessing longer simulation times and larger system sizes compared with atomistic MD simulations. On the other hand, one has to be aware that this approach comes with the cost of reduced accuracy due to the lower resolution. Furthermore, the dynamics of the systems are accelerated due to the smoothed free energy surface. For further information about the coarse-grained approach, see Kmiecik et al.[73] for a general overview and Marrink and Tieleman[74] for a perspective on the MARTINI model. After energy minimization, an NPT simulation of 100 ns was done to adjust the box dimensions. In the latter step, the polymers were kept fixed at their initial position. Production runs were carried out with NVT molecular dynamics simulations for 500 ns for each setup. Here, the CNT was kept fixed at its initial position. The time step was set to 20 fs. In combination with the Verlet neighbor list scheme, a straight cutoff with a cutoff-distance of 11 Å was used. Furthermore, the temperature was controlled with the velocity-rescale thermostat[75] using a coupling constant of 1 ps. To control the pressure in the NPT simulations, the Berendsen barostat with a coupling constant of 12 ps was applied. Furthermore, the compressibility of the system was set to 3 × 10^{-4} bar^{-1}. Freezing of water is a common problem in coarse-grained simulations.[60,76,77] To overcome this problem and decrease the probability of freezing, antifreeze (AF) particles with concentration of 15% with respect to water particles were considered. In addition, a temperature of 310 K was used for the simulations in the NPT and NVT ensembles. The issues related to water freezing and diffusion of water through CNTs with

different lengths and diameters were considered in the ESI (see Section I involving Table S1, Fig. S1 and S2†).

The radius of gyration, R_g, is defined as the mean-squared distance of the polymer beads to their center of mass, r_G, *i.e.*

$$R_g{}^2 = \frac{1}{M} \sum_{i=0}^{N} m_i \langle (r_i - r_G)^2 \rangle \tag{1}$$

where m_i and r_i are the mass and position of the polymer bead i respectively, and M is the total mass of the polymer. R_g was calculated using the VMD visualization program (version 1.9.3).[78] Note that the average R_g values of the different polymers studied below do not exceed $R_g \sim 15$ Å which is much smaller than the simulation box dimensions, thus spurious effects due to the periodic boundary conditions can be excluded.

To characterize the strength of interaction/binding of NPs (polymers) to non-polar environment (CNT), interaction energies E_{int} between polymers and the rest of the system (CNT and water) were calculated as the sum of the Lennard–Jones interactions:

$$E_{int} = \sum_{i<j} 4\varepsilon_{ij} \left[\left(\frac{\sigma_{ij}}{|R_{ij}|} \right)^{12} - \left(\frac{\sigma_{ij}}{|R_{ij}|} \right)^{6} \right] \tag{2}$$

These energies were calculated *via* energy groups using GROMACS tools. The cutoff for the Lennard–Jones interaction was set to 11 Å, which is the standard cutoff used in the MARTINI force field. For the present models, no charged beads were applied. However, it should be emphasized that the electrostatic interactions are involved implicitly within the Lennard–Jones parameters and especially *via* the interaction strength ε.[60] In principle, 10 different interaction levels among polar, non-polar, apolar and charged molecular systems or moieties could be defined based on the ε parameter. GROMACS tools were also used to calculate the partial density profiles of the NP particles along the z-dimension of the CNT (see Fig. 1c and d). Given the full density $\rho(r)$, the partial density is defined as

$$P(z) = \iint \rho(r) \mathrm{d}x \mathrm{d}y \tag{3}$$

For a better comparison between the different polymer types, the resulting partial density distribution $P(z)$ was normalized by its numerically calculated integral along the CNT:

$$\tilde{P}(z) = \frac{P(z)}{\int P(z) \mathrm{d}z} \tag{4}$$

This quantity can be interpreted as a position probability density.

3   Results and discussion

The NPT equilibration simulations produced a density of around 0.86 g cm^{-3} for each investigated system. This deviation mainly comes from the usage of antifreeze-particles. It is a known effect and is caused by the stronger repulsion between

antifreeze and water particles. It is assumed that models are still realistic enough to represent a system at nearly room temperature. It should be noted that all analyses are done with considering only the NVT production trajectories.

3.1   NPs in water

The dependence of the radius of gyration, eqn (1), on the number of monomers N is shown in Fig. 2 for each polymer. Physical properties of the polymers such as hydrophobicity and hydrophilicity can be read off from Fig. 2. For PEO, R_g for a given chain length is larger than for the other polymers. This points to the PEO's hydrophilic nature leading to a more unfolded structure as compared to the hydrophobic PE, PP, and PS which tend to minimize their contact area with a polar solvent. However, one should not take the overall lowest R_g values for PP as an indication of its largest hydrophobicity. Instead, one should also take into account the relatively short bond length and a low mapping compared to *e.g.* PE (see Table S2 in the ESI†). PS, on the other hand, has also a comparable short bond length between beads of its backbone, but shows the largest R_g from the hydrophobic polymers. This is due to the phenyl groups, that increase the occupied volume of the folded PS chain and therefore raise R_g. The degree of hydrophobicity was estimated by calculating interaction energies and radial distribution functions between NPs and water (see Fig. S3 and S4 in the ESI†). From the interaction energy values, one can conclude that PE has the highest hydrophobicity, while PS has the lowest one among the considered hydrophobic polymers.

According to the Flory theory of polymers, R_g is proportional to the number of monomers to the power of the so-called Flory exponent ν.[48] Therefore, the fit function

$$R_g(N) = aN^{\nu} \tag{5}$$

was used to fit the data points shown in Fig. 2 and to determine the Flory exponent of each polymer type. Application of the
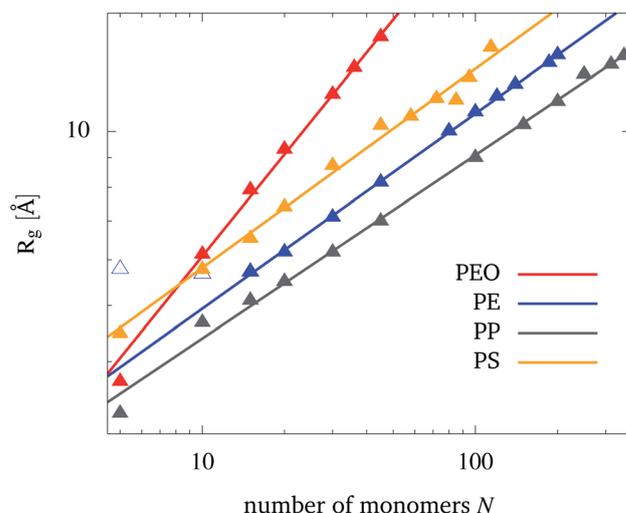

Fig. 2 The dependence of the radius of gyration, R_g, on the number of monomers, N, for the polymers in water (symbols). Also shown is the fit to eqn (5) (straight lines). For PE, the first two data points are excluded from the fit.

Table 1 Calculated fit parameters according to the mean field approach of Flory, for each polymer type. ν is the Flory exponent

	PEO	PE	PP	PS
a [Å]	1.58	2.27	2.11	2.63
ν	0.59	0.34	0.32	0.34

Flory model to coarse-grained polymers is problematic for small chain lengths, where the discretization of the chain has a larger influence on the polymers behavior than the interacting with the solvent. In the present case, this is particularly prominent for PE whose coarse-grained representation has the longest bond length as compared to the other polymers (see Table S2 in the ESI†). Therefore, the first two data points have been excluded form the fit. For the remaining data points the Flory model is clearly confirmed ($R^2 = 0.99$ in all cases). The calculated fit parameters are shown in Table 1.

The Flory exponent makes a statement about the polymer–solvent interaction, especially whether the polymer is in a bad or good solvent. As water is polar, it is a good solvent for PEO and a bad solvent for PE, PP and PS. This can be observed from the calculated Flory exponents. According to the Flory theory for polymers, the Flory exponent is around 0.59, if a polymer is present in a good solvent, while it is around 0.33 if a polymer is present in a bad solvent. From the almost quantitative agreement observed in Table 1, one can conclude that the present coarse-grained model provides a reliable representation of the polymer–solvent interaction. There has been one previous study of PEO in water using the MARTINI force field by Grunewald et al.[61] in which they obtained similar results ($a = 1.81$ and $\nu = 0.58$). The larger value for a is likely due to the different temperature (298.15 K) and antifreeze particle concentration (AF = 10%) used by these authors.

Further, the reliability of the coarse-grained representation for the present modeled polymers in water was tested *versus* an atomistic representation. Specifically, 12 atomistic MD simulations based on the general CHARMM force field[79,80] were performed considering all polymers (PE, PEO, PP and PS), each with three different chain lengths (10, 45 and 100 monomer units). For each case, about 20 ns MD simulation was carried out involving one polymer inside a water box with a density of about 1 g cm^{-3}. The radii of gyration obtained by the CG simulation showed the same trend obtained by the atomistic simulation with a correlation having $R^2 = 0.99$. Moreover, the CG representation showed a good correlation with the atomistic one for the interaction energy values ($R^2 = 0.95$). This overall agreement between the results of both CG and atomistic representations refers to the validity and ability of the CG approach to simulate the present molecular models and especially the NPs interactions with water. For more details, see Section III in the ESI, Fig. S5, S6, Tables S3 and S4.†

3.2 NPs with CNTs in water

3.2.1 Trajectory analysis. In the following, interaction energies are calculated and analyzed in terms of polymer configuration and positioning, *i.e.* in solution as well as at the outer surface and inside the CNT. These positions are realized by choosing different initial conditions as shown in Fig. 1c and d. One should notice, that some polymers (mostly PEO chains) move inside the CNT, which had a starting configuration outside. In the following, results of systems with polymers having radius of gyration R_g of 9 Å in water and with initial conditions outside the CNT are summarized. An example for inside initial conditions for PE is given in Fig. S7 in the ESI.†

During the trajectory, PEO is in a relatively unfolded state (this holds for all R_g values used in this study) with an R_g value not much different from the solution case, see upper panel of Fig. 3. PEO partly sticks at the outer CNT wall (*cf.* middle snapshot), but frequently goes back into solution and returns. Once inside the CNT, PEO prefers to stay directly attached at the inner wall. Furthermore, some polymers go through every of the three introduced positions in one trajectory (in solution, outer walls, inside the CNT).

The interaction energies along the trajectory are shown in Fig. 3 as well. Notice that due to the cutoff for the Lennard–Jones potentials (11 Å) no interaction with the CNT would be
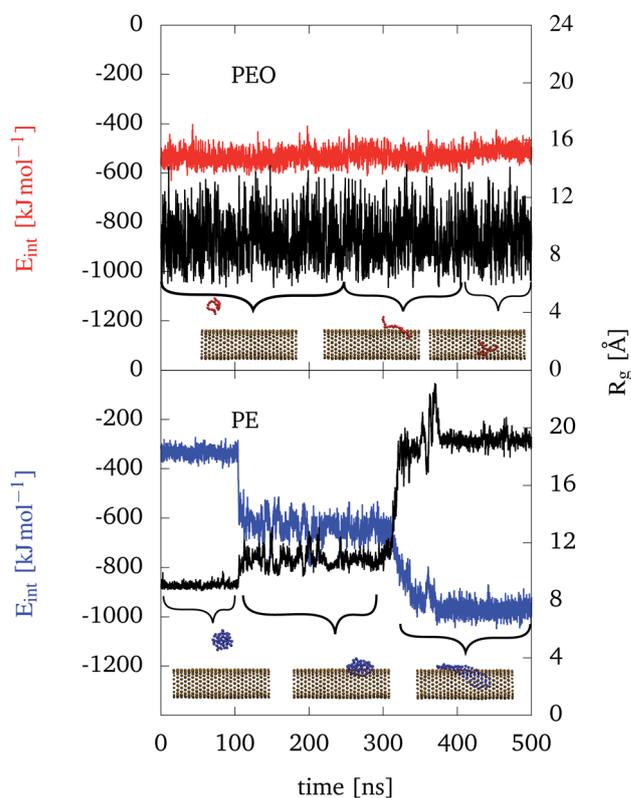
Fig. 3 Interaction energies (red and blue) along the production trajectories for PEO and PE with initially $R_g = 9$ Å. For PE, the line relates to the simulation with the polymer outside the CNT. The interaction energy between the respective polymer and the rest of the system is considered. Furthermore, R_g (black) is plotted for both polymers. The curly brackets denote the time intervals, in which position in the system the respective polymer is found. (For PEO: in solution, at the outer and inner wall of the CNT. For PE: in solution, at the outer wall in configuration A and at the outer wall in configuration B).

observed when PEO is far away from the CNT in solution. However, from the red curve in the upper panel of Fig. 3 we notice that the interaction energy is nearly unchanged along the trajectory, no matter whether PEO is in solution or at the outer wall of the CNT. Once PEO is inside the CNT, the interaction is slightly decreased. Note that in this work, more negative E_{int} implies a stronger interaction. Thus we conclude that the interaction between PEO and the CNT is not much different than with water. The similarity of the two environments is also reflected in the almost unchanged radius of gyration which fluctuates around 9 Å. Of course, for the configurations inside the CNT once should note that R_g is much smaller than the CNT's diameter such that PEO does not have to make significant structural adjustments to go through the CNT.

The situation is rather different for the hydrophobic PE as shown in the lower panel of Fig. 3. In solution PE folds into a sphere like object. In contrast to PEO, once a PE chain adsorbs to the outer wall of the CNT, it stays there and does not go into solution again. Being at the outer wall, two configurations can be distinguished, i.e. a folded (A) and an unfolded one (B). The two configurations can be separated from one another by their different interaction energies and R_g values as seen in Fig. 3.

Regarding the interaction energy between PE and the rest of the system, the blue curve shows its course of time for sticking in an outer wall position. When the polymer is adsorbing at the CNT in the A configuration, the interaction energy drops to around -600 kJ mol^{-1}. When the polymer is changing to configuration B, the interaction energy drops further by -350 kJ mol^{-1}. This increased interaction is due to the increase of the contact area with the hydrophobic CNT as well as with the hydrophilic water in the unfolded state.

Compared to PEO, the interaction of PE with the CNT is much stronger and therefore leads to a more stable adsorbed configuration. Furthermore, the difference in positions (in solution or interacting with the CNT) are more pronounced for PE. As a consequence, PE doesn't change positions (solution, in/outside) in contrast to the hydrophilic PEO.

The differences between configuration A and B for PE are also visible in the time evolution of R_g in Fig. 3. For PE being in solution, R_g is around 9 Å. Then, after adsorbing at the CNT in configuration A, it is fluctuating around 11 Å and when the PE chain is unfolding itself into configuration B, R_g increases to around 19 Å. So, PE maximizes the contact area to the CNT, which significantly increases R_g and also the interaction energy, as discussed above.

Regarding the other two hydrophobic polymers, PP and PS, the following observations can be made from the trajectory data shown in Fig. S8 in the ESI.† Qualitatively, PP behaves like PE, e.g. there are similar configurations A and B although PP is slightly less unfolded in case B as compared with PE. In addition the energy drop when interacting with the CNT is generally weaker. In case of PS, there has been a difference insofar as it doesn't unfold once adsorbed at the outer wall of the CNT (see Fig. S8 in the ESI†). The increase of interaction upon adsorption is relatively modest only. This can be explained by the less flexible structure of PS such that a smaller part of the polymer can directly attach to the CNT (change of R_g is negligible small). PS shows a slight decrease in the interaction energy with the

rest of the system, when being adsorbed at the CNT. This change is less pronounced, when compared to the other hydrophobic polymers PE and PP, but larger compared to PEO. This behavior also reflects the relative strong interaction energy of PS to water (see Fig. S3 in the ESI†), compared to the other hydrophobic polymers.

3.2.2 Interaction energies. In the following, we will provide a more general picture of the interaction between the polymer and the rest of the system. It will cover R_g values (as obtained in solution, cf. Fig. 2) between 6 Å and 10 Å. Interaction energies will be given relative to their values for the polymers in solution E_{sol}. Further, we will distinguish between the adsorption at the outer wall of the CNT (E_{out}) and inside the CNT (E_{in}). For the case of outer wall adsorption we further differentiate between configurations A and B if applicable. The resulting NVT averaged interaction energies are compiled in Fig. 4. In this diagram, more negative values imply a high stability with respect to the polymer in solution.

For the case of PEO, the relative interaction energies are above and close to zero for all chain lengths, no matter whether PEO is inside or adsorbed at the outer wall of the CNT. This confirms the conclusion drawn from Fig. 3, i.e. that there is no preference for PEO to be adsorbed at the CNT. The positive values indicate its hydrophilic character.

The other extreme is PE, which shows in particular noticeable differences with respect to the different configurations (cf.
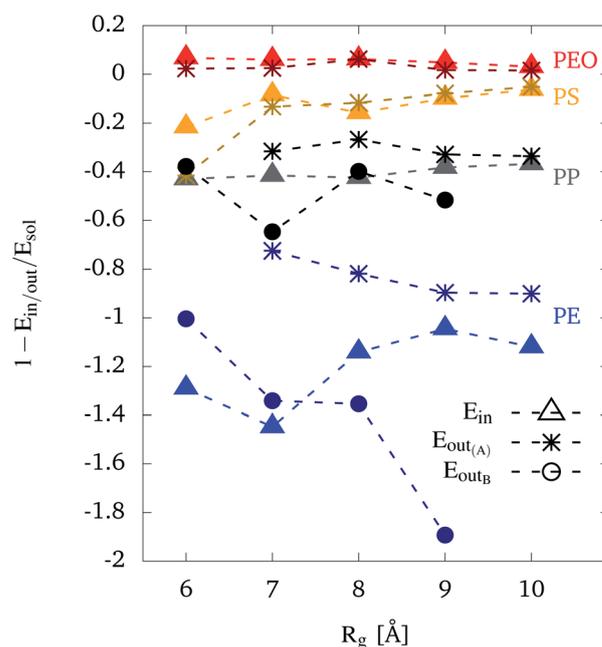
Fig. 4 Interaction energies relative to the bare solvent case as a function of solution phase radius of gyration and configuration. The colors stand for PEO (red), PE (blue), PP (gray) and PS (orange). For each polymer type, Δ denotes the interaction energy (E_{in}), when the polymer is inside the CNT and * refers to the interaction energy ($E_{out_{(A)}}$) at the outer wall of the CNT and for PE and PP, when the polymer is in configuration A. For PE and PP, ○ denotes the interaction energy (E_{out_B}), when the chain is in configuration B. Cases corresponding to missing points were not observed in the production trajectory. For a better visualization data points are connected with dashed lines.

Fig. 3). Values for configuration A at the outer wall are around −0.8, slightly decreasing with increasing R_g. On the other hand, the relative interaction energies for configuration B are strongly decreasing with an increasing R_g. This clearly indicates that with increasing polymer length, the gain in interaction energy due to the higher contact area in the unfolded state outperforms the interaction with water which dominate for the shorter polymers. PE inside the CNT does not show a clear trend, except a minimum at $R_g = 7$ Å. PE (partly) unfolds inside the CNT. Given the size constraint due to the CNT, $R_g = 7$ Å is likely to present an optimum for unfolding and thus increasing the contact area. Compared to configuration B relative interaction energies for PE inside the CNT are lower or similar for a R_g up to $R_g = 7$ Å, but higher for longer polymer chains. All values for PE inside the CNT are lower than for configuration A. Hence, we can conclude that for shorter chain lengths an inside configuration is preferred, whereas long chains tend to unfold in an outer wall configuration.

The behavior of the other hydrophobic polymers, PP and PS, is intermediate between the cases of PEO and PE. Looking at the values for PP, relative interaction energies in configuration A and inside the CNT are approximately constant, around −0.3 and −0.4, respectively. For PP in configuration B, similar or lower values (*e.g.* for $R_g = 7$ Å) are observed, compared to the polymer being inside the CNT. Furthermore, configuration B results in lower values than configuration A. This result is similar to PE, although with a smaller gain in interaction energy. It agrees with the observations from the trajectories, namely that PP does not unfold itself that much when switching from configuration A to B, compared to PE.

Regarding the relative interaction energies for PS, the values are approximately constant around −0.2 to −0.1. Note that PS chains that were adsorbed at the CNT were observed in the folded A configuration only. An exception is the case $R_g = 6$ Å which could also have been counted as B configuration. This explains the deviation between interaction energies at this radius of gyration. Except for this case, all values for PS are higher PP and lower than PEO.

3.3 NPs with functionalized CNTs in water

In the following, we will consider the influence of organic groups placed inside the CNT (as shown in Fig. 1e) on the binding of CNTs to NPs. The analysis will be performed in terms of the partial density $\tilde{P}(z)$ according to eqn (5). Partial densities for all polymers (with $R_g = 7$ Å) and different functionalizations are plotted in Fig. 5. Specifically, partial density profiles are calculated along the z axis of the CNT (see Fig. 1c). Here, $z = 0$ refers to the center of the CNT which the functional groups are placed as well. For each NP-CNT model with a specific functional group, only one simulation was performed by a starting conformation in which the polymer was placed at one CNT end (see Section 2.1.3). In principle, if the simulation started with a mirror configuration (*i.e.* the polymer was placed at the other CNT end), one would have a mirrored partial density profile. For this reason, in the following we are going to discuss the symmetrized partial density profiles, *i.e.* the normalized
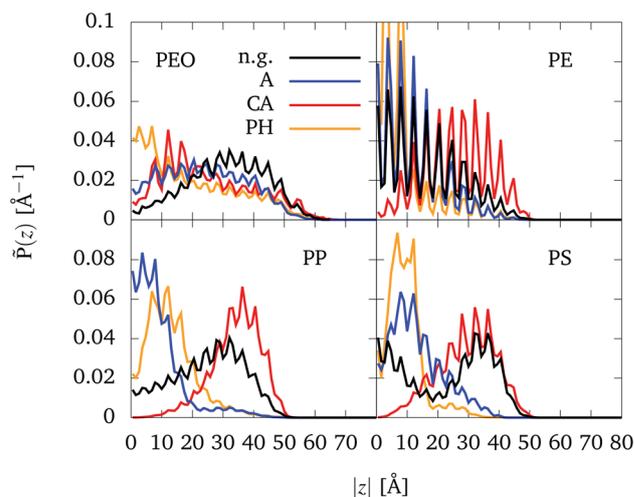

Fig. 5 Normalized partial densities, $\tilde{P}(z)$, for different polymers being (mostly) inside the CNT ($|z| < 50$ Å), depending on the absolute value of the z-coordinate $|z|$. At $z = 0$ the functional groups are situated, *cf.* Fig. 1e. Four different cases are considered: no functional groups (black), alkane chains (blue), carboxylic acid groups (red), and phenyl groups (orange). Note that for PE–PH the two maxima which are out of the scale reach ∼0.16 Å^{-1}.

distribution $(\tilde{P}(z)+\tilde{P}(-z))/2$ along $|z|$. The complete partial density profiles along both negative and positive z values are provided in Fig. S9 in the ESI.†

The distributions show more or less pronounced periodic modulations with a period of about 4.1 Å. This can be explained with the structure of the CNT which consists of rings of beads separated by about 4.07 Å, see Fig. 1b. The beads of the polymers tend to be placed in between the CNT beads.

In case of PEO, no significant differences are visible between the different setups. There is a tendency that a small part of the chain leaves the CNT, which points to slight preference of PEO to be surrounded by water molecules. Moreover, in the cases of alkane and phenyl functionalization, the polymer chain passes $z = 0$ (see Fig. S9 in the ESI†). At first glance, it seems surprising that PEO accumulates at the phenyl groups. However, in the MARTINI force field the π electron density of the phenyl rings is represented by a higher ε value as compared to the alkane chain (2.66 *vs.* 2.53). Note that the interaction area with a phenyl group is also higher, because they are described by three beads. Further note that the interaction with the carboxylic acid groups is masked by the presence of water, attracted to that group.

The distributions for PE do not show significant differences with respect to the four setups. PE stays away from the center to avoid close contact with the hydrophilic carboxylic acid groups. In contrast the hydrophobic alkane chains and phenyl groups attract PE which therefore shows a higher density towards the middle of the CNT as compared to the bare CNT case. Since the bulky phenyl groups present an obstacle for PE it cannot easily penetrate through $z = 0$ and thus shows a higher density as compared with the case of alkane chains.

For the other hydrophobic polymers, PP and PS, the behavior concerning the hydrophilic carboxylic acid groups is similar to the case of PE. For PP and PS, one notices that the oscillations

are less pronounced due to the shorter bond lengths (see Table S2 in the ESI†), *i.e.* its beads do not strictly fill out every of the spaces between the rings of the CNT. The same result can be obtained for PEO, also because it is less attracted by the CNT walls and therefore less influenced by its periodic potential. In absence of functional groups, PP and PS tend to stay closer to their initial positions as compared to PE. On the one hand side, this looks reasonable considering the different bulkiness, *cf.* Fig. 1a. On the other hand side, it could be that even the 500 ns trajectory doesn't fully sample the available configuration space.

In accordance with chemical intuition, the hydrophobic polymers have a preference for the hydrophobic functional groups and avoid hydrophilic ones. Water plays a role in controlling this behavior. Water particles are repelled by the hydrophobic functional groups, thus allowing the hydrophobic polymers to reach the region close the center more easily. On the other hand, water particles are attracted by carboxylic acid groups, making it harder for the hydrophobic polymers to access this region.

The structural changes of the polymers inside the functionalized CNT are addressed in Fig. 6. Here, R_g is plotted as a function of the distance between the CNT and polymer centers of masses. Only the cases PE and PP are considered here, which according to Fig. 5 show pronounced differences (for PEO and PS, see Fig. S10 in the ESI†).

For PE, the mean values of R_g (black lines) for the systems with alkane chains and phenyl groups are higher than for the carboxylic acid and bare CNT cases. This increase in R_g correlates with the attraction to the hydrophobic functional groups. Therefore, one can conclude that interaction with functional groups of similar (hydrophobic/hydrophilic) behavior leads to a slight unfolding of the polymers. In all cases, the polymer partly unfolds inside the CNT as compared to the solvated case ($R_g = 7$ Å). Concerning the spread of R_g values, the bare CNT and the case of alkane chains do not behave much different. For the system with the phenyl groups, data points are less spread. This comes due to an arrangement of PE to a ring structure (see Fig. S11 in the ESI†), in which it stays for more than the half of the simulation time. In this position, PE stays relatively fixed and close to the phenyl groups. It is the only case where such a special arrangement was observed. This might be only possible due to the phenyl groups occupying more space inside the CNT and therefore leading to a significant obstacle to the movement of the polymers. Also notable is the shift of the distribution towards larger δ_{CNT-NP} for the case of the carboxylic acid groups, which is caused by the repulsion of PE, or in general hydrophobic polymers (including PP) to the carboxylic acid groups. This can be observed as well in the distributions of Fig. 5.

Compared to PE, the distribution for PP is more compact. Also the pronounced tendency of PE to unfold inside the CNT is not observed for PP. This can be explained with the shorter bond length of PP in the coarse-grained picture, which allows it to stay more compact than PE. Regarding the atomistic picture, this comes due to the slightly more ramified structure caused by the methyl groups of PP. Notable changes are only observed for the system with phenyl groups. During the simulation, PP passes the phenyl groups to end up in a more stretched configuration leading to higher R_g values close to the center of the CNT.

Due to the final propagation time, one has to be careful with interpretation of the absolute numbers. Comparing the scenarios, however, the differences between functional groups and polymer types are becoming obvious. This holds in particular if one notes that PE and PP behave rather similar in water (*cf.* Fig. 2).

Fig. 6 R_g of polymers inside the CNT, depending on the center of mass distance δ_{CNT-NP} between the respective polymer and the CNT. Colors blue and gray relate to PE and PP, respectively. For each polymer, four different systems are investigated, with CNT in absence of functional groups (first row), CNT and alkane chains (second row), CNT and carboxylic acid groups (third row), and CNT and phenyl groups (fourth row) in the system (average R_g – black line).

4 Conclusions

Coarse-grained molecular dynamics simulations were performed to address the interaction of NPs with hydrophobic parts of macromolecular organic soil constituents such as
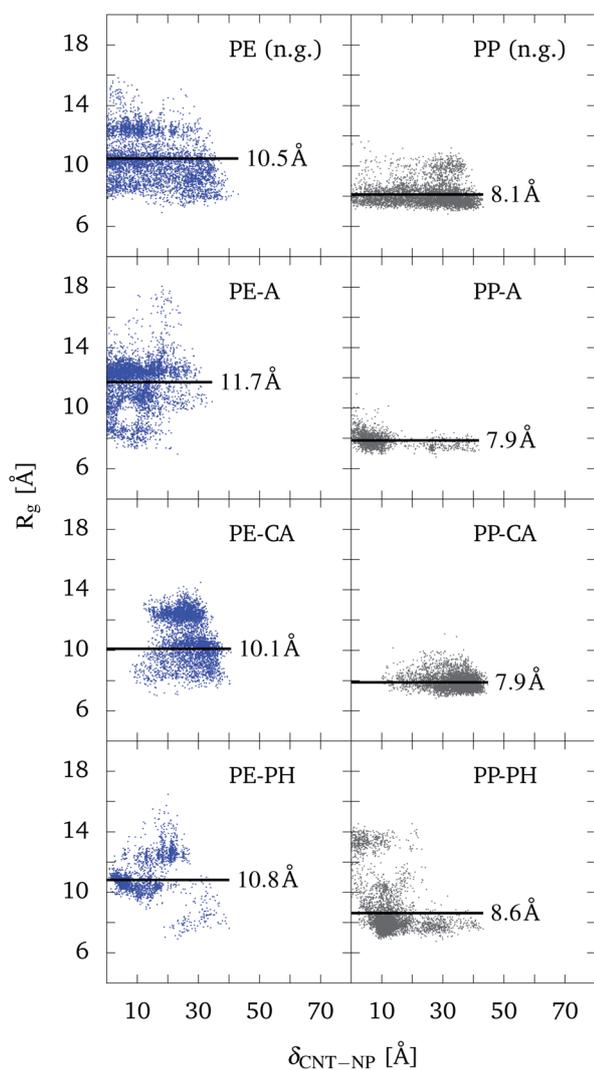
surfaces and functionalized cavities. NPs were modeled by four representative polymers, *i.e.* the hydrophilic PEO and the hydrophobic PE, PP, and PS. For the hydrophobic surfaces/functionalized cavities, a carbon nanotube model was taken.

First, the behavior of the NPs in water was characterized by means of their radii of gyration. Results were found to be in agreement with Flory theory, thus validating the parametrization of the MARTINI force field for the particular models.

Next, the interaction of the polymers with a bare CNT in water was investigated. Based on the hydrophobicity/hydrophilicity of the polymers, different adsorption behaviors were observed. PEO as a hydrophilic polymer prefers solvation over adsorption either at the outer wall or inside, whereas the hydrophobic polymers stayed at the CNT, once adsorbed. In general, independent of the radius of gyration, PE showed the strongest interaction with the CNT, followed by PP and PS. For PE and PP, two configurations at the outer CNT wall were observed, which differ in the degree of unfolding. Unfolding increases the contact area with the CNT which leads to a more stable configuration.

The hydrophobicity of the CNT cavity was modified by introducing different hydrophilic and hydrophobic functional groups, *i.e.* alkane, phenyl and carboxylic acid groups. While PEO was not much influenced by the cavity and in fact it partly moved out during the simulation, a strong dependence of the behavior on the combination functional group/polymer was observed for the hydrophobic cases. Compared to the solution, PE shows the largest increase of the radius of gyration, followed by PP and PS. All three polymers tend to avoid the hydrophilic carboxylic acid groups. On the other hand, they are attracted by the hydrophobic groups and accumulate close to their positions inside the CNT.

Although these results are not unexpected, they can be viewed as a first step towards a mechanistic understanding of a variety of processes, *e.g.* in environmental soil chemistry, water treatment, and biochemistry. Correlating the present results to soil chemistry points to the critical role of the hydrophobicity in controlling the binding process of NPs in soil. In fact, the investigated models can be seen as capturing generic aspects of the interaction between NPs and soil organic matter (SOM). SOM is characterized by its overall hydrophobicity, apart from certain functional groups. The CNT in the present work acts as an effective hydrophobic environment for NPs. Due to the similarity of the chemical properties, conclusions can be made on how NPs might behave in SOM. Hydrophobic NPs could have a higher tendency to accumulate in soil and especially soil with high content of hydrophobic SOM. Furthermore, the results indicate that SOM cavities/voids could play an influential role in accumulation, *i.e.* immobilization, of NPs in soil. Moreover, the chemical nature of functional groups being present at SOM active surfaces and/or inside SOM cavities/voids plays a role by increasing/decreasing the extent of that accumulation. In a next step, refinement of the model can be envisioned, *e.g.* to include more complex SOM models such as macromolecules[66,81,82] or to incorporate organic pollutants, heavy metals[83,84] and other compounds[85] bound to the NPs.

It is interesting to note that due to the well defined and unique physicochemical properties of CNTs, they have been used recently in water treatment technologies and especially to remove organic pollutants, *e.g.*, dyes, pharmaceuticals/drugs, pesticides, phenols and aromatic amines. The present results are in accord with the literature in showing that the hydrophobicity of CNTs and modification/decoration of their surfaces with organic functional groups plays an important role in controlling the adsorption/binding/accumulation of organic compounds into outer and inner surfaces of CNTs.[86–89] Therefore, fine tuning and modification for the hydrophobic character of CNTs with organic functional groups could enhance the adsorption capacity of CNTs to remove specific organic pollutants from aqueous solutions and waste water. Thus, the present contribution introduces a very fundamental model approaching the idea behind adsorption and removal of organic compounds by CNTs.

Conflicts of interest

There are no conflicts to declare.

References

1 K. N. Fotopoulou and H. K. Karapanagioti, *The Handbook of Environmental Chemistry*, Springer International Publishing, 2017, pp. 71–92.

2 J. Gigault, B. Pedrono, B. Maxit and A. T. Halle, *Environ. Sci.: Nano*, 2016, **3**, 346–350.

3 B. S. S. Ramasamy and S. Palanisamy, *Environ. Sci. Pollut. Res.*, 2021, DOI: 10.1007/s11356-021-14883-6.

4 S. S. Sadri and R. C. Thompson, *Mar. Pollut. Bull.*, 2014, **81**, 55–60.

5 M. Zbyszewski, P. L. Corcoran and A. Hockin, *J. Great Lakes Res.*, 2014, **40**, 288–299.

6 C. M. Free, O. P. Jensen, S. A. Mason, M. Eriksen, N. J. Williamson and B. Boldgiv, *Mar. Pollut. Bull.*, 2014, **85**, 156–163.

7 M. R. Gregory, *Philos. Trans. R. Soc., B*, 2009, **364**, 2013–2025.

8 A. L. Andrady, *Mar. Pollut. Bull.*, 2011, **62**, 1596–1605.

9 A. A. de Souza Machado, W. Kloas, C. Zarfl, S. Hempel and M. C. Rillig, *GCB Bioenergy*, 2018, **24**, 1405–1416.

10 M. C. Rillig, L. Ziersch and S. Hempel, *Sci. Rep.*, 2017, **7**, 1362.

11 M. Bläsing and W. Amelung, *Sci. Total Environ.*, 2018, **612**, 422–435.

12 A. A. Horton, A. Walton, D. J. Spurgeon, E. Lahive and C. Svendsen, *Sci. Total Environ.*, 2017, **586**, 127–141.

13 J. Wang, X. Liu, Y. Li, T. Powell, X. Wang, G. Wang and P. Zhang, *Sci. Total Environ.*, 2019, **691**, 848–857.

14 N. B. Hartmann, S. Rist, J. Bodin, L. H. Jensen, S. N. Schmidt, P. Mayer, A. Meibom and A. Baun, *Integr. Environ. Assess. Manage.*, 2017, **13**, 488–493.

15 S. Wagner and T. Reemtsma, *Nat. Nanotechnol.*, 2019, **14**, 300–301.

16 O. S. Alimi, J. F. Budarz, L. M. Hernandez and N. Tufenkji, *Environ. Sci. Technol.*, 2018, **52**, 1704–1724.

17 A. Käppler, D. Fischer, S. Oberbeckmann, G. Schernewski, M. Labrenz, K.-J. Eichhorn and B. Voit, *Anal. Bioanal. Chem.*, 2016, **408**, 8377–8391.

18 G. Zhang and Y. Liu, *Sci. Total Environ.*, 2018, **642**, 12–20.

19 J. N. Möller, M. G. J. Löder and C. Laforsch, *Environ. Sci. Technol.*, 2020, **54**, 2078–2090.

20 K. Khosravi-Katuli, E. Prato, G. Lofrano, M. Guida, G. Vale and G. Libralato, *Environ. Sci. Pollut. Res.*, 2017, **24**, 17326–17346.

21 M. F. L. De Volder, S. H. Tawfick, R. H. Baughman and A. J. Hart, *Science*, 2013, **339**, 535–539.

22 P.-H. Hermes, M.-P. Gabriela, V.-R. Ileana, C. Fusaro, L.-V. Fernando, M.-A. Mariana, C. Padilla-Rodríguez and F.-L. Fabián, *Green Nanoparticles*, ed. J. K. Patra, L. F. Fraceto, G. Das and E. V. R. Campos, Springer International Publishing, Cham, 2020, pp. 77–115.

23 W. Tang, T. Yan, F. Wang, J. Yang, J. Wu, J. Wang, T. Yue and Z. Li, *Carbon*, 2019, **147**, 295–302.

24 V. Erady, R. J. Mascarenhas, A. K. Satpati, A. K. Bhakta, Z. Mekhalif, J. Delhalle and D. A, *Microchem. J.*, 2019, **146**, 73–82.

25 Y. Bakytkarim, S. Tursynbolat, Q. Zeng, J. Huang and L. Wang, *J. Electroanal. Chem.*, 2019, **841**, 45–50.

26 Y. Liu, S. Wang, W. Lan and W. Qin, *Int. J. Biol. Macromol.*, 2019, **121**, 1329–1336.

27 M. V. Khodakovskaya, B.-S. Kim, J. N. Kim, M. Alimohammadi, E. Dervishi, T. Mustafa and C. E. Cerniglia, *Small*, 2012, **9**, 115–123.

28 X. Ma, J. Geiser-Lee, Y. Deng and A. Kolmakov, *Sci. Total Environ.*, 2010, **408**, 3053–3061.

29 P. Begum, R. Ikhtiari, B. Fugetsu, M. Matsuoka, T. Akasaka and F. Watari, *Appl. Surf. Sci.*, 2012, **262**, 120–124.

30 H. Hyung and J.-H. Kim, *Environ. Sci. Technol.*, 2008, **42**, 4416–4421.

31 M. Ateia, O. G. Apul, Y. Shimizu, A. Muflihah, C. Yoshimura and T. Karanfil, *Environ. Sci. Technol.*, 2017, **51**, 7101–7110.

32 M. Engel and B. Chefetz, *Adv. Colloid Interface Sci.*, 2019, **271**, 101993.

33 A. Bakir, S. J. Rowland and R. C. Thompson, *Mar. Pollut. Bull.*, 2012, **64**, 2782–2789.

34 T. Hüffer and T. Hofmann, *Environ. Pollut.*, 2016, **214**, 194–201.

35 S. Seidensticker, P. Grathwohl, J. Lamprecht and C. Zarfl, *Environ. Sci. Eur.*, 2018, **30**, 30.

36 K. Yang, L. Zhu and B. Xing, *Environ. Sci. Technol.*, 2006, **40**, 1855–1861.

37 C.-J. M. Chin, L.-C. Shih, H.-J. Tsai and T.-K. Liu, *Carbon*, 2007, **45**, 1254–1260.

38 W. Chen, L. Duan, L. Wang and D. Zhu, *Environ. Sci. Technol.*, 2008, **42**, 6862–6868.

39 D. Petrov, D. Tunega, M. H. Gerzabek and C. Oostenbrink, *Environ. Sci. Technol.*, 2017, **51**, 5414–5424.

40 A. A. Ahmed, S. Thiele-Bruhn, S. G. Aziz, R. H. Hilal, S. A. Elroby, A. O. Al-Youbi, P. Leinweber and O. Kühn, *Sci. Total Environ.*, 2015, **508**, 276–287.

41 E. Slonkina and A. B. Kolomeisky, *J. Chem. Phys.*, 2003, **118**, 7112–7118.

42 H.-P. Hsu and P. Grassberger, *J. Chem. Phys.*, 2004, **120**, 2034–2041.

43 W. Reisner, K. J. Morton, R. Riehn, Y. M. Wang, Z. Yu, M. Rosen, J. C. Sturm, S. Y. Chou, E. Frey and R. H. Austin, *Phys. Rev. Lett.*, 2005, **94**, 196101.

44 W. Sparreboom, A. van den Berg and J. C. T. Eijkel, *Nat. Nanotechnol.*, 2009, **4**, 713–720.

45 G. O. Ibáñez-García and P. Goldstein-Menache, *Soft Matter*, 2012, **8**, 8666.

46 B.-Y. Ha and Y. Jung, *Soft Matter*, 2015, **11**, 2333–2352.

47 M. P. Taylor, *Macromolecules*, 2017, **50**, 6967–6976.

48 M. Rubinstein and R. Colby, *Polymer Physics*, OUP Oxford, 2003.

49 Q. Cao and M. Bachmann, *Soft Matter*, 2017, **13**, 600–607.

50 S. Jun and A. Wright, *Nat. Rev. Microbiol.*, 2010, **8**, 600–607.

51 F. Müller-Plathe, *ChemPhysChem*, 2002, **3**, 754–769.

52 J. Baschnagel, K. Binder, P. Doruker, A. A. Gusev, O. Hahn, K. Kremer, W. L. Mattice, F. Müller-Plathe, M. Murat, W. Paul, S. Santos, U. W. Suter and V. Tries, *Viscoelasticity, Atomistic Models, Statistical Chemistry*, Springer Berlin Heidelberg, Berlin, Heidelberg, 2000, vol. 152, pp. 41–156.

53 J. Zhao, J.-W. Jiang, L. Wang, W. Guo and T. Rabczuk, *J. Mech. Phys. Solids*, 2014, **71**, 197–218.

54 S. Cranford and M. Buehler, *Multiscale Modeling*, ed. P. Derosa and T. Cagin, CRC Press, 2010, pp. 13–34.

55 R. Geyer, J. R. Jambeck and K. L. Law, *Sci. Adv.*, 2017, **3**, e1700782.

56 S. Piehl, A. Leibner, M. G. J. Löder, R. Dris, C. Bogner and C. Laforsch, *Sci. Rep.*, 2018, **8**, 17950.

57 F. A. E. Lots, P. Behrens, M. G. Vijver, A. A. Horton and T. Bosker, *Mar. Pollut. Bull.*, 2017, **123**, 219–226.

58 D. He, Y. Luo, S. Lu, M. Liu, Y. Song and L. Lei, *TrAC, Trends Anal. Chem.*, 2018, **109**, 163–172.

59 J.-J. Guo, X.-P. Huang, L. Xiang, Y.-Z. Wang, Y.-W. Li, H. Li, Q.-Y. Cai, C.-H. Mo and M.-H. Wong, *Environ. Int.*, 2020, **137**, 105263.

60 S. J. Marrink, H. J. Risselada, S. Yefimov, D. P. Tieleman and A. H. de Vries, *J. Phys. Chem. B*, 2007, **111**, 7812–7824.

61 F. Grunewald, G. Rossi, A. H. de Vries, S. J. Marrink and L. Monticelli, *J. Phys. Chem. B*, 2018, **122**, 7436–7449.

62 E. Panizon, D. Bochicchio, L. Monticelli and G. Rossi, *J. Phys. Chem. B*, 2015, **119**, 8209–8216.

63 G. Rossi, L. Monticelli, S. R. Puisto, I. Vattulainen and T. Ala-Nissila, *Soft Matter*, 2011, **7**, 698–708.

64 L. Martínez, R. Andrade, E. G. Birgin and J. M. Martínez, *J. Comput. Chem.*, 2009, **30**, 2157–2164.

65 M. Vögele, J. Köfinger and G. Hummer, *Faraday Discuss.*, 2018, **209**, 341–358.

66 H. R. Schulten and M. Schnitzer, *Naturwissenschaften*, 1993, **80**, 29–30.

67 J. Kubicki and C. Trout, *Geochemical and Hydrological Reactivity of Heavy Metals in Soils*, ed. H. Magdi Selim and W. Kingery, CRC Press, 2003.

68 A. J. A. Aquino, D. Tunega, G. Haberhauer, M. H. Gerzabek and H. Lischka, *Eur. J. Soil Sci.*, 2007, **58**, 889–899.

69 A. J. A. Aquino, D. Tunega, H. Pašalić, G. E. Schaumann, G. Haberhauer, M. H. Gerzabek and H. Lischka, *Environ. Sci. Technol.*, 2011, **45**, 8411–8419.

70 A. A. Ahmed, O. Kühn and P. Leinweber, *Sci. Total Environ.*, 2012, **441**, 151–158.

71 A. A. Ahmed, O. Kühn, S. G. Aziz, R. H. Hilal and P. Leinweber, *Sci. Total Environ.*, 2014, **476–477**, 98–106.

72 E. Lindahl, M. J. Abraham, B. Hess and D. van der Spoel*GROMACS 2020.3 Manual*, Zenodo, 2020.

73 S. Kmiecik, D. Gront, M. Kolinski, L. Wieteska, A. E. Dawid and A. Kolinski, *Chem. Rev.*, 2016, **116**, 7898–7936.

74 S. J. Marrink and D. P. Tieleman, *Chem. Soc. Rev.*, 2013, **42**, 6801.

75 G. Bussi, D. Donadio and M. Parrinello, *J. Chem. Phys.*, 2007, **126**, 014101.

76 S. J. Marrink, A. H. de Vries and A. E. Mark, *J. Phys. Chem. B*, 2004, **108**, 750–760.

77 S. J. Marrink, X. Periole, D. P. Tieleman and A. H. de Vries, *Phys. Chem. Chem. Phys.*, 2010, **12**, 2254.

78 W. Humphrey, A. Dalke and K. Schulten, *J. Mol. Graphics*, 1996, **14**, 33–38.

79 J. Lee, X. Cheng, J. M. Swails, M. S. Yeom, P. K. Eastman, J. A. Lemkul, S. Wei, J. Buckner, J. C. Jeong, Y. Qi, S. Jo, V. S. Pande, D. A. Case, C. L. Brooks, A. D. MacKerell, J. B. Klauda and W. Im, *J. Chem. Theory Comput.*, 2015, **12**, 405–413.

80 K. Vanommeslaeghe, E. Hatcher, C. Acharya, S. Kundu, S. Zhong, J. Shim, E. Darian, O. Guvench, P. Lopes, I. Vorobyov and A. D. Mackerell, *J. Comput. Chem.*, 2010, **31**, 671–690.

81 H.-R. Schulten and P. Leinweber, *Biol. Fertil. Soils*, 2000, **30**, 399–432.

82 H. Feng, H. Zhang, H. Cao, Y. Sun, A. Zhang and J. Fu, *Environ. Sci. Technol.*, 2018, **52**, 14228–14234.

83 J. Cheng, J. Liang, L. Dong, J. Chai, N. Zhao, S. Ullah, H. Wang, D. Zhang, S. Imtiaz, G. Shan and G. Zheng, *RSC Adv.*, 2018, **8**, 40813–40822.

84 J. Liang, J. Li, X. Li, K. Liu, L. Wu and G. Shan, *Sep. Purif. Technol.*, 2020, **230**, 115874.

85 G. B. Braun, K. N. Sugahara, O. M. Yu, V. R. Kotamraju, T. Mölder, A. M. Lowy, E. Ruoslahti and T. Teesalu, *J. Controlled Release*, 2016, **232**, 188–195.

86 V. K. Gupta, R. Kumar, A. Nayak, T. A. Saleh and M. Barakat, *Adv. Colloid Interface Sci.*, 2013, **193–194**, 24–34.

87 W. Wu, K. Yang, W. Chen, W. Wang, J. Zhang, D. Lin and B. Xing, *Water Res.*, 2016, **88**, 492–501.

88 J.-G. Yu, X.-H. Zhao, H. Yang, X.-H. Chen, Q. Yang, L.-Y. Yu, J.-H. Jiang and X.-Q. Chen, *Sci. Total Environ.*, 2014, **482–483**, 241–251.

89 X. Qu, P. J. Alvarez and Q. Li, *Water Res.*, 2013, **47**, 3931–3946.